NUMERICAL SIMULATION AND PROCESS OPTIMIZATION OF VACUUM INVESTMENT CASTING FOR Be–Al ALLOYS

Z. H. Wang, J. Wang, L. B. Yu, J. Wu, M. Wang, and B. Su
Institute of Materials, China Academy of Engineering Physics, Jiangyou, China

Abstract

Be–Al alloy castings are widely used in aviation, aerospace and marine industries due to their excellent comprehensive properties. To improve the quality of products, vacuum investment casting of a bracket casting of Be–Al alloys was simulated using the finite-element method and the evolution of the flow field and temperature field as well as the formation of shrinkage porosity were simulated. The simulated results of positions of shrinkage porosity agreed well with the experimental results. The optimized casting parameter with ceramic shell preheat temperature of 500 °C and pouring temperature of 1300 °C was determined by numerical simulation. After the process optimization, a high quality Be–Al alloy casting was successfully produced by pouring once.

Keywords: numerical simulation, Be–Al alloys, investment casting, casting defects, finite-element modeling

Introduction

Beryllium–aluminium (Be–Al) alloys, has many excellent properties such as lightweight, high specific stiffness and good thermal stability, and it is estimated to be the next-generation aerial and aerospace structures materials.[1,2] Currently the investment casting process, which could produce fine casts with little or no machining, is the preferred method of producing Be–Al alloys. However, due to large freezing range, high latent heat of fusion, and low capability of heat diffusion, shrinkage cavity and porosity occur frequently in Be–Al alloy castings.[3,4] Therefore, how to select the appropriate casting process and technological parameters to produce high quality Be–Al alloy castings is a problem to overcome.

Be–Al alloys are expensive and also toxic, which limits the experimental research. In recent years, with the advancements of computer technology, numerical modeling and simulation have been widely used as a powerful tool to make a description of the solidification process.[5–8] Many researchers have investigated the solidification process using commercially available casting simulation software. It can be used to design a casting process using less energy and can predict how to reduce defects of cast products. It is also helpful to shorten the trial period and reduce the producing cost.[9–16]

In this study, a commercially available process simulation software,[12–17] ProCAST, was employed to investigate the investment casting process of a bracket casting of Be–38 wt%Al alloy. Flow field and temperature field during filling and solidification process were simulated, and the formation of shrinkage porosity was predicted. To validate the simulated results, the actual casting experiments were carried out and the defects appearing in casting parts was also analyzed. Finally, the casting process parameters were redesigned and optimized based on the numerical simulation.

Experimental Procedures

Mathematical Model

In this study, the flow of liquid metal is assumed to be incompressible Newtonian fluid and the governing equations.[10,14] Heat transfer equation, Continuity equation and Navier–stokes equation, at the filling and solidification stages were numerically solved by ProCAST software.[17] Niyama criterion, which is the most widely used criterion function of metal casting, was utilized to predict the shrinkage porosity in this study. The Niyama criterion, Ny, is a local thermal parameter defined as follows:[11,15]
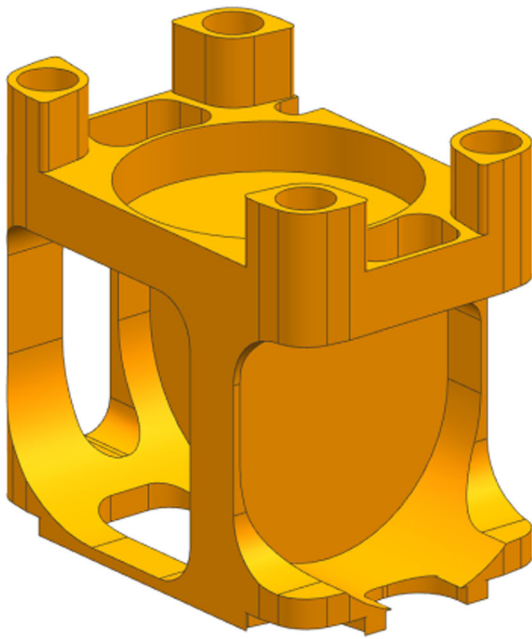
Figure 1. Three-dimensional model of the bracket casting of Be–Al alloys.

$$Ny = \frac{G}{(v_c)^{1/2}} \qquad \text{Eqn. 1}$$

where G is temperature gradient, and v_c is cooling rate.

Geometric Model and Parameters Setting of Simulation

The three-dimensional model of the bracket casting of Be–Al alloys was designed by UG software, as shown in Figure 1. Three-dimensional size of the bracket is 142 mm × 100 mm × 145 mm, and wall thickness of the casting changes from about 7 to 18 mm. The model was imported into the finite-element-based simulation software, which was used to simulate filling and solidification

process of the investment casting. It contains 44,172 nodes and 162,747 elements. The nominal composition of actual casting material was Be–38 wt%Al and the ceramic mold material was mainly zircon sand. Thermophysical parameters of Be–Al alloys and ceramic mold material required in the simulation are listed in Table 1, which was obtained from the literature[1–4] and material database of ProCAST. In addition, reverse technology was employed to obtain thermophysical parameters of the Be–Al alloys at high temperature, and the technical details of the reverse technology can be seen in Reference 18. The heat transfer coefficient of casting/shell, shell/gas environment was set as 1000 W/(m²·K), 50 W/(m²·K), respectively.

The Actual Casting Experiments

Investment casting process of Be–Al alloys includes pattern manufacturing, ceramic shell building, pattern removal, pouring and finishing. The polystyrene (PS) pattern was produced by selective laser sintering (SLS), which is an additive manufacturing method that uses a powder bed fusion process to build 3D parts, as shown in Figure 2. The AFS 450 SLS sintering system (equipped with 50 W CO_2 Laser) used in the experiment was made by Beijing longyuan Automated Fabrication System Co., Ltd. in China. Polystyrene powders with a range of particle sizes from 50 to 97 μm were used as SLS material. Sintering parameters of the PS powder are listed in Table 2. The SLS pattern was reinforced by infiltrating with wax and the obtained pattern which mainly consists of plastic and wax was used for the ceramic shell building.

The pattern was coated with ceramic layer through dipping into refractory slurry and stuccoed with coarse sand followed with drying. Zircon sand (particle size 150 μm) was used as the stuccoing material of surface layer and mullite sand (particle size 250–500 μm) was used as the stuccoing material of back layer. The refractory slurry was prepared

Table 1. Thermophysical Parameters of Alloy and Mold Material

| Material property	Materials	Values	Sources
Conductivity (W·m⁻¹·K⁻¹)	Be–38 wt%Al	60–185	Reference 1–4
	Ceramic mold	0.83–0.97	ProCAST software
Density (kg·m⁻³)	Be–38 wt%Al	2050–2150	Reference 1–4
	Ceramic mold	2780	ProCAST software
Specific heat (kJ·kg⁻¹·K⁻¹)	Be–38 wt%Al	1.55	Reference 1–4
	Ceramic mold	0.44–0.85	ProCAST software
Liquidus (K)	Be–38 wt%Al	1355	Reference 2
	Ceramic mold	–	–
Solidus (K)	Be–38 wt%Al	919	Reference 3
	Ceramic mold	–	–
Viscosity (Pa·s)	Be–38 wt%Al	$(1.17–1.83) \times 10^{-3}$	–
	Ceramic Mold	–	–
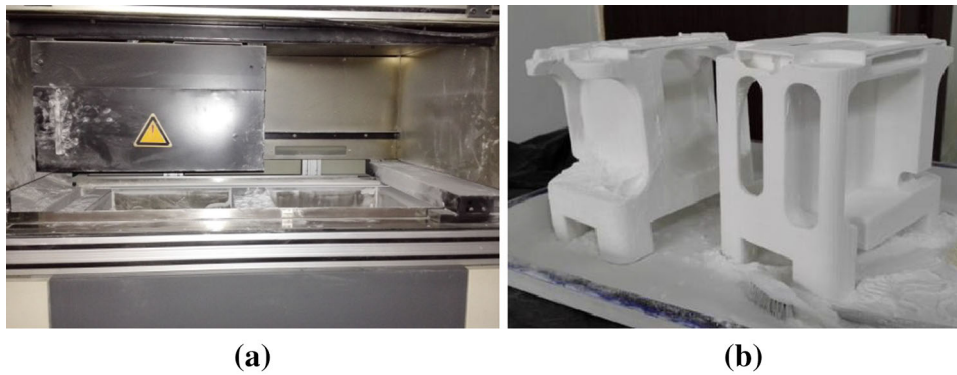
Figure 2. The PS pattern was produced by additive manufacturing method. (a) SLS sintering system and (b) PS pattern.

Table 2. Sintering Parameters of the PS Powder

Parameters	Value
Layer thickness (mm)	0.15
Scanning speed (mm·s^{-1})	1800
Beam spot size (mm)	0.05–0.2
Preheating temperature of the build chamber (°C)	95

in accordance with the order of zirconium sol → additives → ZrO_2 powder, and the stirring speed was controlled at 30–50 rpm/min. The slurry was obtained with the viscosity of about 30–40 s and the suspension rate of approximately 80%. The next layers of ceramic mold were prepared in a similar manner. Six ceramic layers were produced and the thickness of the ceramic shell was approximately 10 mm. The time for drying between each layer was 24 h. The wax materials in the pattern was removed at 150 °C for 30 min via autoclave dewaxing, and the remaining pattern material was removed during the initial preheating of the ceramic shell mold. The obtained ceramic shell mold was preheated for 30 min at 300 °C to remove moisture and to burn off residual pattern material, baked for 4 h at 900 °C to sinter the ceramic, then cooled to room temperature in the furnace. The residual ash was cleaned with hot water. To discharge the gas from the cavity and avoid the shrinkage porosity, a dozen vent holes with the diameter of 5 mm were set at top of shell during the ceramic shell building. Ceramic shell mold and the position of the vent holes are shown in Figure 3.

The actual pouring experiment was carried out using 30 kg vacuum induction melting furnace. The ceramic shell mold was placed in the heating chamber of the furnace and preheated at the temperature of 600 °C. Be–38 wt%Al alloy was melted at 1320 °C for 15 min, and the vacuum was 0.8 Pa. The pouring temperature of molten metal was about 1250 °C, and the filling time was 6–8 s. When the pouring of the liquid metal was finished, the ceramic shell
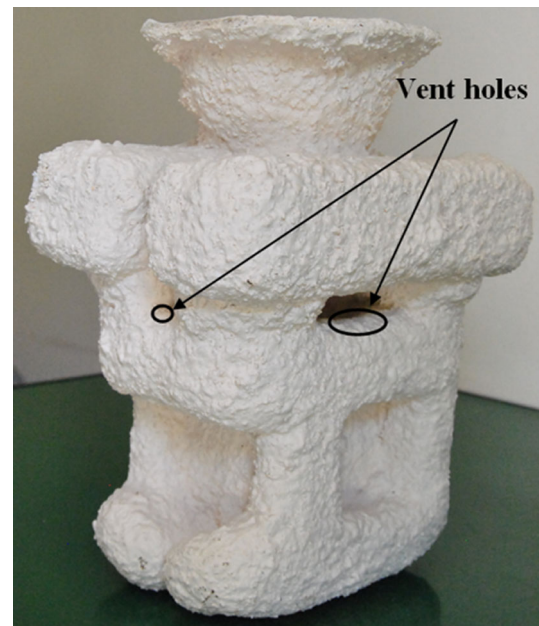

Figure 3. Ceramic shell mold and the position of vent holes.

mold was withdrawn from the heating chamber to the cooling chamber of the furnace, which was about 40 °C. Finally, the ceramic shell mold was broken with a pneumatic hammer to get casting products after cooling. The pouring experiments were repeated twice under the same parameter to ensure the accuracy of the experimental results.

Results and Discussion

Figure 4 shows the simulation results of filling processes of the Be–Al alloy casting. It indicates the positions of the molten metal front in the cavity at different filling time. It clearly shows that the liquid metal flows through the sprue and runner system and into the cavity of the casting. When the filling time is 1.5 s, the liquid metal reaches the bottom of the cavity with a temperature of about 940 °C. When the
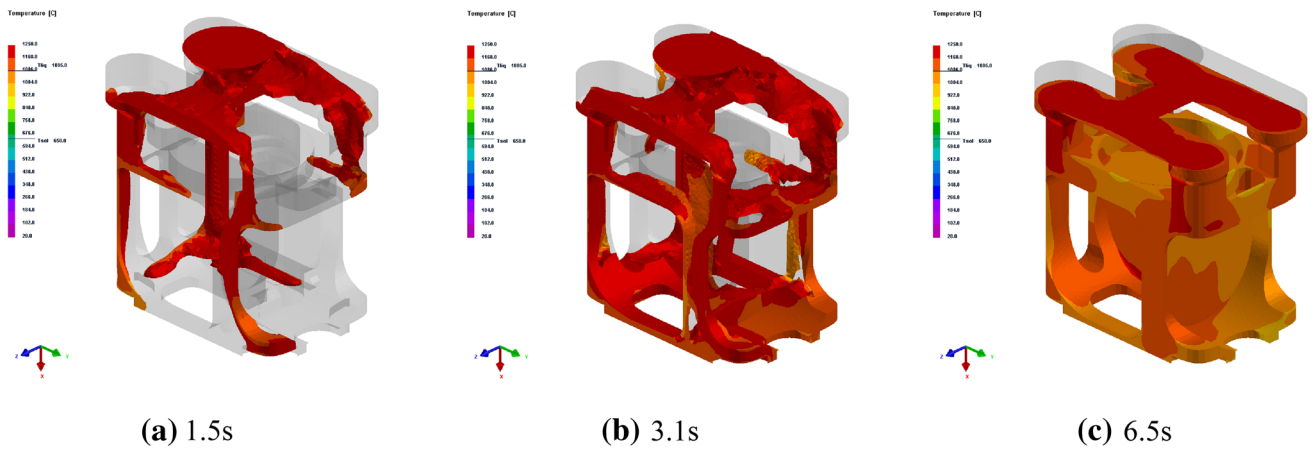
(a) 1.5s   **(b)** 3.1s   **(c)** 6.5s

Figure 4. The evolution of the filling state at different times.

filling time is 3.1 s, the cavity is 50% filled. When the filling time is 6.5 s, the cavity is fully filled. It is found that the filling process is smooth and the design of gating system is reasonable.

Once the mold cavity is completely filled, solidification simulation is followed. The simulated results can explore the reasons how shrinkage porosity defects formed. Figure 5 shows the temperature field during different solidification states, and Figure 6 shows solidification time of different position of the casting. Several locations (P1–P4) were selected to investigate the temperature distribution and variation at different locations in the casting, as shown in Figure 6. Figure 7 shows the cooling curves of the selected locations inside the casting during solidification process. It can be that the thin wall position (P3) of the casting cool faster than other parts, and shrinkage porosity defects may be formed between P2 and P4 because the feeding paths are cut off. Figure 8 shows the predicted shrinkage porosity of the casting. It shows that shrinkage porosity defects may be formed at the location below the
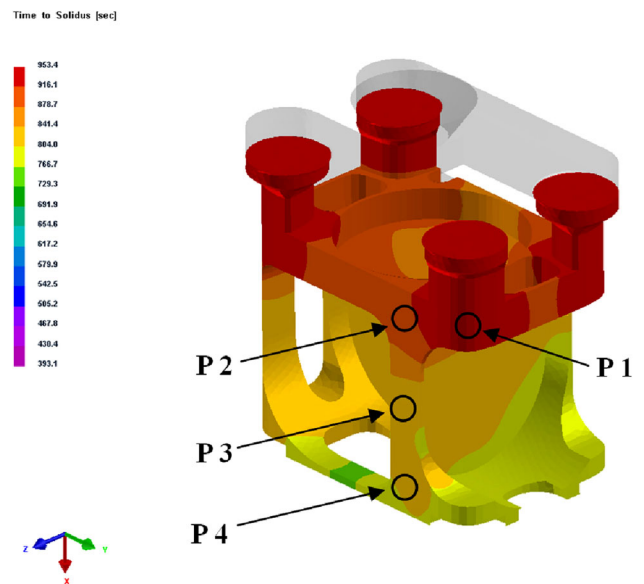

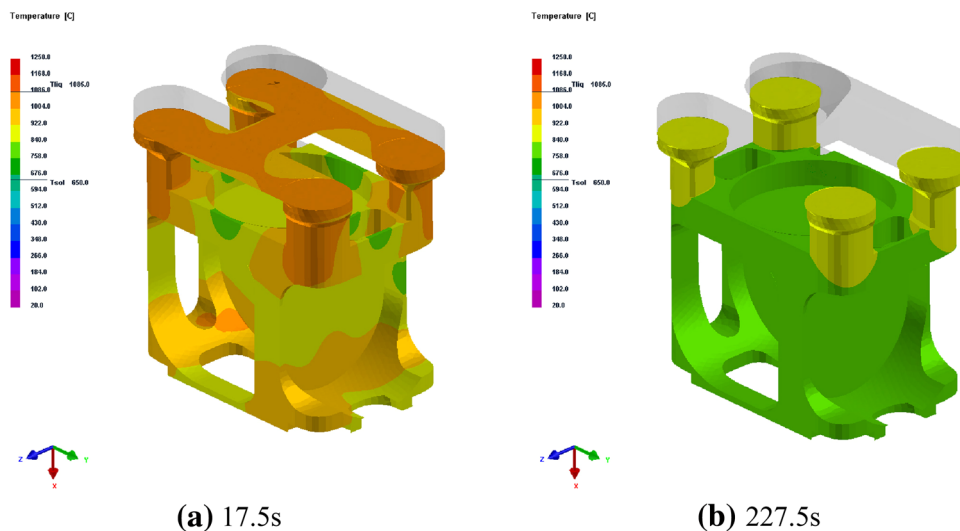*Figure 6. Solidification time of different position of the casting.*

(a) 17.5s   **(b)** 227.5s

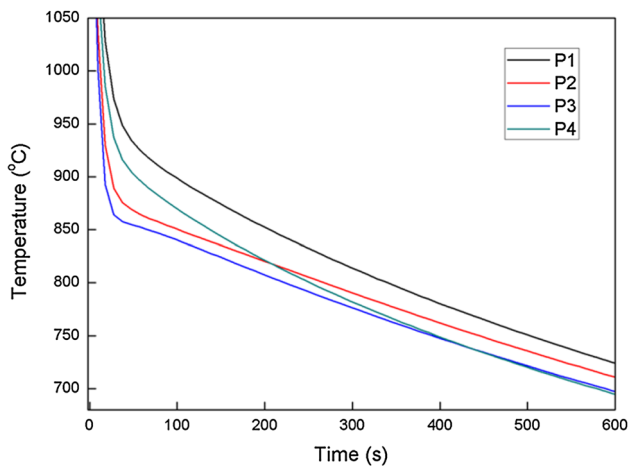*Figure 5. Temperature field during solidification.*

Figure 7. The temperature change curves at different locations inside the casting during casting. (P1–P4 are different locations selected to investigate the temperature distribution and variation).
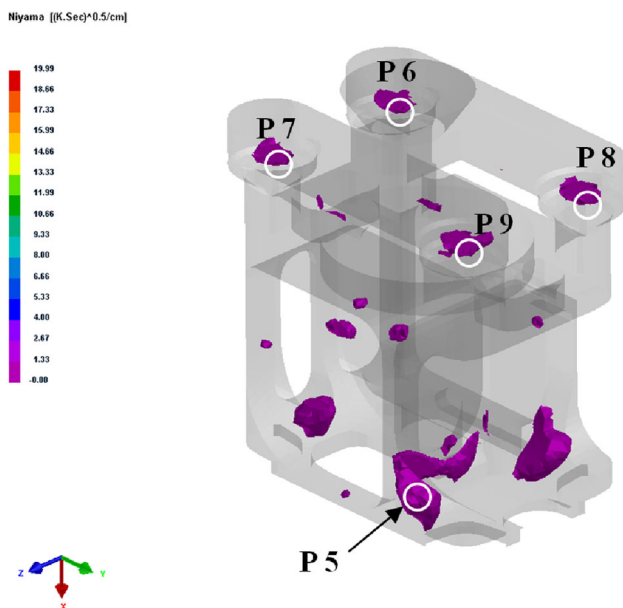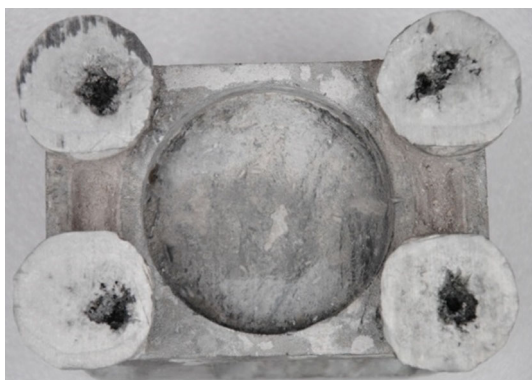

Figure 8. The predicted shrinkage defects.

Figure 9. Shrinkage defects existed below the risers in the Be–Al alloy casting.

riser besides the lower part of the casting. Figure 9 shows the shrinkage defects below the risers after the risers were cut off, which agrees well with the predicted shrinkage porosity below the risers (P6–P9) in Figure 8.

To investigate the shrinkage porosity distributed in the casting, samples were taken from the Be–Al alloy casting and detected by micro computed tomography (micro-CT). The sample size was 39 mm×5 mm×1 mm, and the total material volume was 195 mm^3. Radiographic images were acquired at spatial resolution of 5 μm and reconstructed by VGStudio Max$^®$ 2.0 software. 3D characterization and distribution of the shrinkage porosity in the samples were obtained. Optical images were recorded on an Olympus (DSX-500) optical microscope. Figure 10 displays the shrinkage porosity and microstructure of the sample taken from the position where the shrinkage porosity is predicted (P5 in Figure 8). It can be seen that shrinkage porosity defects exist around the thin wall position of the Be–Al alloy casting. The experimental and analytical results show that total volume of the shrinkage porosity in Figure 10b is about 19.75 mm^3 and the shrinkage porosity fraction of the sample is 10.13%. Maximum volume of the shrinkage porosity is about 6.26 mm^3. The simulated result for the shrinkage porosity defects is in good agreement with the actual industrial castings.

Due to large freezing range of Be–Al alloys, shrinkage porosity occurs frequently in Be–Al alloy castings and it is difficult to be prevented by realizing sequential solidification. Increasing cooling rate during solidification is beneficial to refine the grain structure and improve the density of the alloys, and it can be useful to enhance the feeding capacity of liquid metal because the growth of dendrite can be inhibited. The shrinkage porosity in Be–Al alloy casting is probably decreased by controlling the cooling rate of liquid metal. To prevent the shrinkage porosity defects, the casting technology was optimized according to the above analysis. The detailed optimizing technical methods include improving feeding ability by increasing the pouring temperature, refining the grain structure by increasing the cooling rate of liquid metal in solidification. In this work, appropriate reduction of the shell preheat temperature was done to increase the cooling rate of the liquid metal. The optimum parameters of investment casting process of Be–38 wt%Al alloy were chosen based on the simulation, which were with ceramic shell preheat temperature of 500 °C and pouring temperature of 1300 °C. Meanwhile, the casting after pouring was cooled using liquid nitrogen in the cooling chamber of the furnace. Figure 11 shows the simulated result of shrinkage porosity defects with the optimized processing parameters. Figure 12 displays the shrinkage porosity and microstructure of the sample taken from the casting in the same position as shown in Figure 10 with the optimum parameters. The experimental and analytical results show that total volume of the shrinkage porosity is about 5.56 mm^3 and the shrinkage porosity
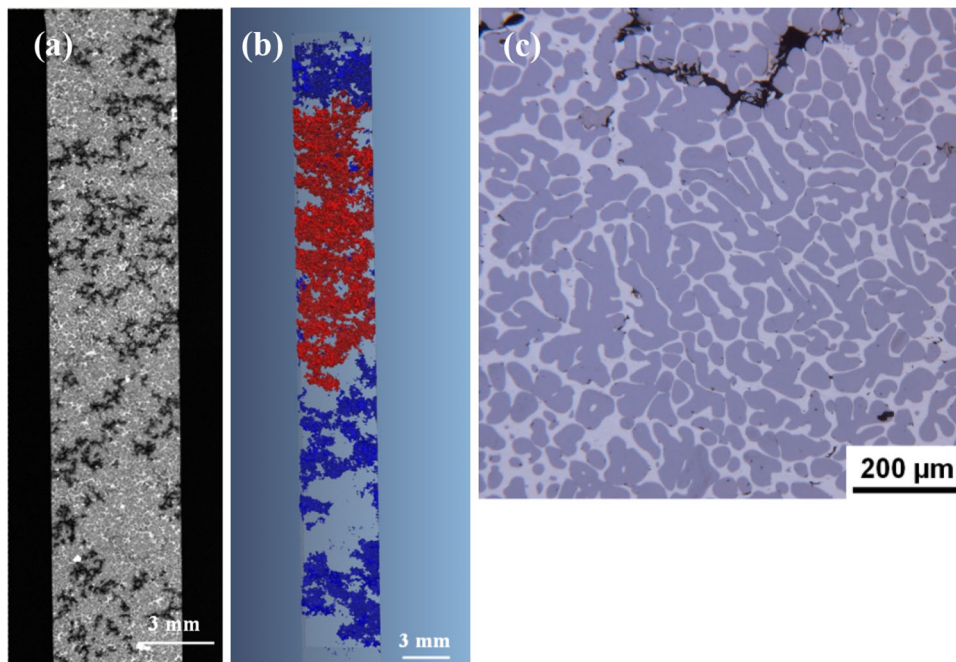
Figure 10. Solidified structure of Be–38 wt%Al alloy. (a) 2D slice and (b) 3D view of shrinkage porosity, (c) microstructure observed by OM.
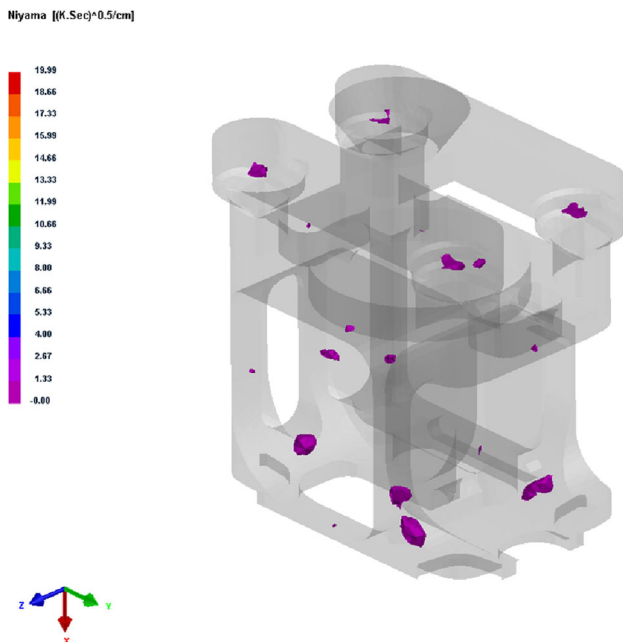

Figure 11. The predicted shrinkage defects with optimized processing parameters.

fraction of the sample is 2.85%, and maximum volume of the shrinkage porosity is 1.32 mm³. The experimental and simulated results show that the optimized processing parameters can reduce the shrinkage porosity in the casting, and it was confirmed by the actual production testing.

Conclusions

The numerical simulation of vacuum investment casting of Be–38 wt%Al alloy was carried out using the finite element method. The flow field and temperature field as well as the formation of shrinkage porosity were simulated. The actual casting experiments were carried out and the shrinkage porosity appeared in casting parts was analyzed. The main conclusions are as follows:

1. Simulated results of positions of the molten metal front in the cavity at different filling time have revealed that the filling process is smooth and the preliminary design of gating system is reasonable. When the filling time is 3.1 s, the cavity is 50% filled. When the filling time is 6.5 s, the cavity is fully filled. The whole filling time of the casting is 6.5 s.

2. The formation of shrinkage porosity defects of the Be–Al alloy casting was predicted. Microstructure and shrinkage porosity of the casting were analyzed using OM and micro-CT. The simulated results are in good agreement with the experimental results.

3. The optimum parameters of vacuum investment casting of Be–38 wt%Al alloy can be obtained according to the simulation results, which are with ceramic shell preheat temperature of 500 °C and pouring temperature of 1300 °C.
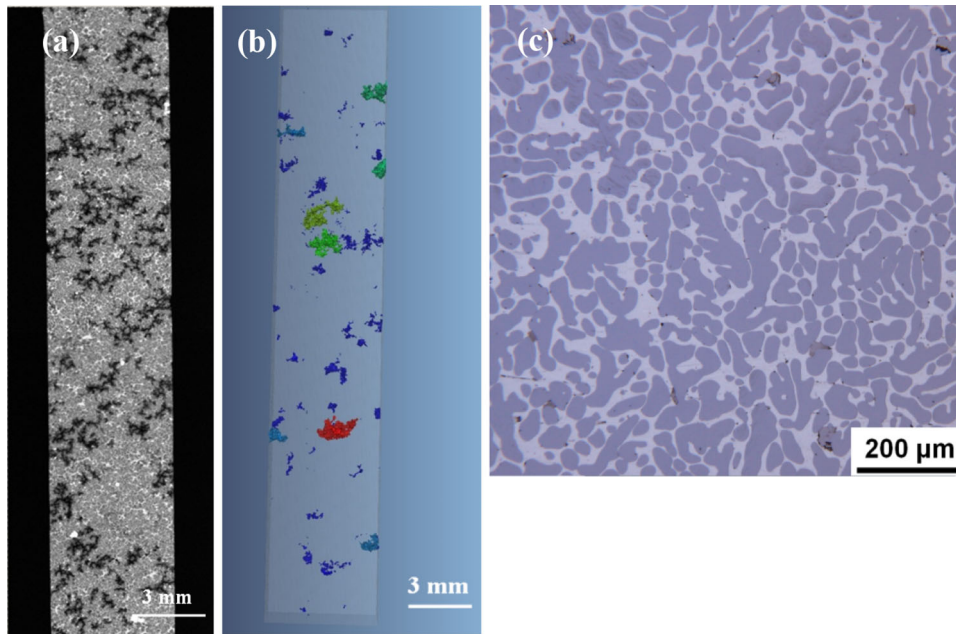
Figure 12. *Solidified structure of Be–38 wt%Al alloy with the optimum parameters. (a) 2D slice and (b) 3D view of shrinkage porosity, (c) microstructure observed by OM.*

Acknowledgements

REFERENCES

1. X.N. Liu, S.G. Ma, Study and application of AlBe alloy. Chin. J. Rare Metals **27**(1), 62–65 (2003)
2. W. Speer, S.E. Omar, Application of aluminum-beryllium composite for structural aerospace component. Eng. Fail. Anal. **11**(6), 895–902 (2004)
3. J.W. Elmer, M.J. Aziz, L.E. Tanner et al., Formation of bands of ultrafine beryllium particles during rapid solidification of Al–Be alloy: modeling and direct observation. Acta Metall. Mater. **42**(4), 1065–1080 (1994)
4. D. Carter, M. Bourke, Neutron diffraction study of the deformation behavior of beryllium-aluminum composites. Acta Mater. **48**(11), 2885–2900 (2000)
5. M. Rappaz, C.A. Gandin, Probabilistic modeling of microstructure formation in solidification processes. Acta Metall. Mater. **41**(2), 345–360 (1993)
6. L. Nastac, Numerical modeling of solidification morphologies and segregation patterns in cast dendritic alloys. Acta Mater. **47**(17), 4253–4262 (1999)
7. F. Shehata, M. Abd-Elhamid, Computer aided foundry die-design. Mater. Des. **24**(8), 577–583 (2003)
8. L. Beltran-Sanchez, D.M. Stefanescu, A quantitative dendrite growth model and analysis of stability concepts. Metall. Mater. Trans. A **35**(8), 2471–2485 (2004)
9. B.C. Liu, S.M. Xiong, Q.Y. Xu, Study on macro- and micro modeling of the solidification process of aluminum shape casting. Metall. Mater. Trans. B **38**(4), 525–532 (2007)
10. G.F. Mi, X.Y. Liu, K.F. Wang, H.Z. Fu, Numerical simulation of low pressure die-casting aluminum wheel. China Foundry **6**(1), 48–52 (2009)
11. I. Khaled, Prediction of shrinkage porosity in Ti-46Al-8Nb tilt-casting using the Niyama criterion function. Int. J. Metalcast. **7**(4), 35–42 (2013)
12. Y. Fang, J. Hu, J.X. Zhou et al., Numerical simulation of filling and solidification in exhaust manifold investment casting. Int. J. Metalcast. **8**(4), 39–45 (2014)
13. J.L. Li, R.S. Chen, Y.Q. Ma, W. Ke, Characterization and prediction of microporosity defect in sand cast WE54 alloy castings. J. Mater. Sci. Technol. **30**(10), 991–997 (2014)
14. L. Yang, L.H. Chai, Y.F. Liang, Numerical simulation and experimental verification of gravity and centrifugal investment casting low pressure turbine blades for high Nb–TiAl alloy. Intermetallics **66**, 149–155 (2015)
15. S.Y. Zhang, J.S. Li, H.C. Kou et al., Numerical modeling and experiment of counter-gravity casting for titanium alloys. Int. J. Adv. Manuf. Technol. **85**(5–8), 1877–1884 (2016)

16. M.Y. Hu, J.J. Cai, W.L. Sun et al., Diecasting simulation and process optimization of an A356 aluminum alloy polishing plate. Int. J. Metalcast. **10**(3), 315–321 (2016)

17. ProCAST User's Manual & Technical Reference. America: ESI Software Inc., 2007

18. Q. Tian, W.G. Wang, J.X. Zhou et al., Application of reverse thermophysical parameters technology in lost foam casting ductile casting. Spec. Cast. Nonferr. Alloys **35**(3), 288–291 (2015)